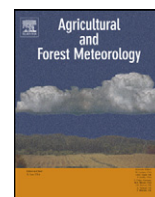Contents lists available at ScienceDirect

Agricultural and Forest Meteorology

journal homepage: www.elsevier.com/locate/agrformet

Forest understory soil temperatures and heat flux calculated using a Fourier model and scaled using a digital camera

Eric A. Graham [a,*], Yeung Lam [b], Eric M. Yuen [a]

[a] *Center for Embedded Networked Sensing, University of California, Los Angeles, 3563 Boelter Hall, Los Angeles, CA 90095-1596, USA*
[b] *Electrical Engineering Department, University of California, Los Angeles, CA 90095-1594, USA*

ARTICLE INFO

ABSTRACT

The characterization of the solar radiation environment under a forest canopy is important for both understanding temperature-dependent biological processes and validating energy balance models. A modified sinusoidal model of soil heat conductivity was used to estimate subsurface temperature and heat flux from the uneven but periodic solar heating of the soil surface due to sun flecks from a forest canopy. Using a mobile sensor platform with an infrared thermometer along an 11 m transect, a sunfleck model of soil surface temperature was tested using soil surface temperature maxima, air temperatures, and photodiodes placed on the soil surface to measure sunflecks. A pan-tilt-zoom digital camera on a 10 m tower above the site was then used to capture a time series of panoramic images of sunflecks reflected from the soil surface and to scale the sunfleck temperature model to a wide area. Finally, this image-based model of surface temperatures was combined with the modified sinusoidal model for heat conduction to estimate soil subsurface temperatures and heat flux over a wide area due to sunflecks from a forest canopy.

© 2010 Elsevier B.V. All rights reserved.

1. Introduction

Soil temperature strongly influences a wide range of biological, CO_2-producing processes including soil microbial activity and root metabolism and affects plant distributions on both large (e.g., Körner and Paulsen, 2004) and small scales (e.g., Schob et al., 2009). Measurements or estimates of soil temperature are also necessary components for estimating local and continental carbon and energy budgets and for calculating evaporative fluxes (Zheng et al., 1993; Gaumont-Guay et al., 2009). It has long been recognized that a variety of factors influence soil temperature, including climate, topography, above-ground vegetation, and soil physical characteristics (Balisky and Burton, 1995; Geiger et al., 2003). Because multiple factors influence soil surface heating, traditional *in situ* sensors may be inadequate for measuring the large spatial and temporal heterogeneity created by a forest canopy.

Most models for estimating soil temperature are based on simplified, bare-soil, or agricultural conditions (e.g., Gonzalez-Dugo et al., 2009; Saito and Simunek, 2009), although there are numerous efforts that include the influence of natural vegetation (e.g., Paul et al., 2004; Bond-Lamberty et al., 2005). Models for soil temperature and heat flux also vary in complexity from estimations of soil temperature based on readily available meteorological measurements

(e.g., Weiss and Hays, 2005) to more complex and physics-based models requiring more specific measurements (e.g., Romano and Giudici, 2009).

Sinusoidal soil temperature models that assume periodic temperature fluctuations and are parameterized with simple meteorological measurements are particularly attractive due to their ease of calculation and minimal data requirements (Paul et al., 2004; Droulia et al., 2009). However, such models can provide unsatisfactory results because they assume soil homogeneity and ignore the spatiotemporal temperature variations caused by overstory shading (Hardy et al., 2004; Bond-Lamberty et al., 2005). A standard method of converting a complex signal into a set of more manageable sinusoidal signals is the Fourier transform, which when used in conjunction with sinusoidal heat conduction models, provides an elegant approach to modeling periodic but uneven subsurface soil temperatures (Van Wijk and de Vries, 1966).

Digital cameras and data storage have become increasingly affordable and hardware more easily integrated into systems for ecological data collection (Hamilton et al., 2007; Rundel et al., 2009). Image analysis from environmental studies, for instance for plant phenology detection, has primarily involved simple color transformations and analysis (Graham et al., 2009; Richardson et al., 2009). The application of digital cameras to the detection of sunfleck patterns on a soil surface requires similarly simple image processing procedures and can be analogous to that for detection of canopy parameters used in hemispherical canopy photography, a robust and well-documented method using a binary threshold-

---

* Corresponding author. Tel.: +1 310 825 2643; fax: +1 310 206 3053.
E-mail address: egraham@cens.ucla.edu (E.A. Graham).

ing of images (Ishida, 2004; Cescatti, 2007). Where hemispherical canopy photography and its analysis can be concerned with predicting the amount of light that strikes the point at which the photograph was taken, a downwardly facing camera system that can recognize sunflecks on the soil surface can be used to monitor a much greater number of points over a large area but at the loss of the predictive power for each location.

Our objective was to combine a sunfleck model of soil surface temperature with a modified sinusoidal model for estimating subsurface soil temperatures to examine the effects of the uneven but periodic solar heating of the soil due to a forest canopy. The sinusoidal model was modified to better deal with subsurface soil heterogeneity. Because sunflecks can be captured as reflected light using a downwardly facing camera, a second objective was to spatially scale these models using a digital pan-tilt-zoom camera. Specifically, we first verified that a modified sinusoidal model could be used to predict subsurface temperature of an uneven but periodic surface temperature signal in the field. Next we constructed and tested a simple model of soil surface temperature based on sunfleck occurrence, maximum observed surface temperature, and air temperature. Then we applied the two models to a sequence of images captured of the soil surface under a forest canopy by a digital camera to spatially scale the soil surface and subsurface temperature estimates.

2. Materials and methods

2.1. Field site

The University of California James Reserve (www.jamesreserve.edu) is located in the San Jacinto Mountains of southern California (33°48′30″N, 116°46′40″W) at 1658 m elevation in a mixed conifer and hardwood forest with a perennial mountain stream. The area receives a mean of 485 mm precipitation annually. The area at which soil surface temperature measurements were taken is a forest gap 645 m^2 in area, as determined by the extent of the unobstructed view of the installed camera system. The middle of the gap has a site openness of 47%, as determined by the percentage of open sky seen from beneath a forest canopy using the analysis of a hemispherical canopy photograph (Gap Light Analyzer, Simon Fraser University, Canada).

Bulk density of the mineral soil, determined from 50 g samples taken just below the leaf litter at the James Reserve near the experimental transect within the forest gap was 1.21 ± 0.13 g m^{-3} ($n = 7$; mean $\pm$ SD). The soil in the bulk density samples was comprised of $77.5 \pm 10.6\%$ sand, $13.2 \pm 6.1\%$ clay, and $9.2 \pm 4.8\%$ silt, with $0.9 \pm 0.6\%$ organic matter contained within those fractions. During July, the soil was essentially dry from the surface to a depth of 8 cm. In March, the volumetric water content of the soil, measured by nearby dielectric sensors (EC-10, Decagon Devices, Pullman, WA, USA), was 0.02 m^3 H$_2$O m^{-3} at 2 cm and 0.09 m^3 m^{-3} at 8 cm; the average volumetric soil water content between the surface and 8 cm depth in March was estimated at 0.04 m^3 m^{-3}. In the laboratory, the volumetric heat capacity (C) and thermal conductivity (λ) were determined for dry soil from the site using the heat pulse method with home-built probes that were calibrated in both air and an aqueous gel with known C and λ, following Nusier and Abu-Hamdeh (2003). Both C and λ of a moist soil was then calculated from the values obtained from a dry soil ($C_{dry} = 1.41$ MJ m^{-3} °C^{-1}; $\lambda_{dry} = 0.62$ W m^{-1} °C^{-1}) by assuming that the apparent C and λ of any soil are due to the sum of separate values of the components of the soil, including the air and water fractions. Then, using the bulk density, we substituted the C and λ of air for that of water to 0.04 m^3 m^{-3} to determine for the moist soil C_{wet} of 1.60 MJ m^{-3} °C^{-1}.

2.2. Surface and subsurface measurement system

The networked infomechanical systems (NIMS) family of cable-based robotic systems, developed at the Department of Electrical Engineering, University of California, Los Angeles (UCLA), includes a rapidly deployable system (Jordan et al., 2007) that has been used for multiple environmental monitoring applications (Harmon et al., 2007; Caron et al., 2008; Graham et al., 2009). In this deployment, the NIMS system support cable was secured to two trees on the side of the forest gap and the motor control unit was attached to a wireless Ethernet bridge for remote control and programming of the system.

A surface scan of temperatures along the 11 m long NIMS transect involved moving the payload of sensors in 0.25 m increments, at which point the system dwelled for 30 s for sensor equilibration, then movement to the next location commenced. Data were captured continuously for 36 h for each measurement period by a datalogger (23X, Campbell Scientific, Logan, UT, USA). Data from a second datalogger (CR7, Campbell Scientific) connected to fixed sensors were collected simultaneously. Data were remotely archived in an open source database (MySQL Inc., Cupertino, CA, USA) with a custom front-end designed to facilitate the sharing of streaming sensor data (SensorBase, www.sensorbase.org; Chang et al., 2006).

Micrometeorological sensors on the NIMS shuttle included a downwardly facing infrared thermometer (Model 4000.3ZL, Everest Interscience Inc., Tucson, AZ, USA) to measure soil surface temperature. An emissivity of 0.9 was used for temperature conversion. Fixed sensors were clustered in four locations on the transect, at 1.75, 5, 7, and 9 m. Buried sensors included copper-constantan thermocouples (0.3 mm diameter) buried at 2, 8, and 16 cm depth and four self-calibrating heat flux plates (HFP01SC-L, Hukseflux Thermal Sensors B.V., Delft, The Netherlands) located at a depth of 8 cm. Depths refer to depths in mineral soil and do not include the thickness of the leaf litter layer, which were 3.2 ± 1.4 cm thick at position 1.75 m, 4.8 ± 2.6 cm at position 5 m, 3.9 ± 2.7 cm at position 7 m, and 2.6 ± 1.6 cm at position 9 m (values are mean SD; $n = 4$ at each location). Surface soil sensors included copper-constantan thermocouples and calibrated, upwardly facing gallium arsenide phosphide photodiodes (Hamamatsu, Bridgewater, NJ) in the same location as the buried sensors.

A dried and a wetted soil treatment were included within 3 m of the middle of the NIMS transect for energy balance comparisons (Qiu et al., 1998). Soil was previously excavated in approximately 10 cm layers to a depth of 0.5 m in an area without vegetation for each treatment and for the dried treatment each layer was spread on a plastic tarp and allowed to dry for 24 h. For both treatments, each layer was then sequentially placed into a rigid cylinder 30 cm in diameter and 36 cm deep that had an aluminum base to allow for vertical heat transfer through the cylinder (Qiu et al., 1998). Each layer was sequentially tamped down to approximate the original bulk density before excavating and a thin leaf litter layer, similar to the surrounding area, was spread over the soil surface of each treatment. Each treatment had a heat flux plate placed at 8 cm below the mineral soil and a thermocouple at 8 and 2 cm depths. An additional, stationary infrared thermometer was alternately placed approximately 20 cm above the soil surface to measure the temperature of each cylinder of soil during measurements made by NIMS.

2.3. Camera and image analysis

Images were captured using a pan-tilt-zoom (PTZ) networked video camera (Model VB-C50iR, Canon U.S.A., Lake Success, New York) mounted on a 10 m fiberglass tower at the James Reserve and connected to a local area network using Wi-fi. Images were collected at two different zooms, near maximum magnification

Table 1
Attenuation (d_1 in Eq. (2)) and delay (d_2 in Eq. (2)) depths calculated using the attenuation of the amplitude and the phase shift of the measured temperature maxima at the surface (of either bare soil or leaf litter surface) and with depth for two treatments (wet or dry) and two locations along the NIMS transect; values are means ± SD (n = 2 d for both bare wet and for dry soil with added litter; n = 11 d for all other locations).

Soil type	Surface to 2 cm		Surface to 8 cm		2–8 cm		8–16 cm	
	Attenuation (d_1; cm)	Delay (d_2; cm)	Attenuation (d_1; cm)	Delay (d_2; cm)	Attenuation (d_1; cm)	Delay (d_2; cm)	Attenuation (d_1; cm)	Delay (d_2; cm)
Wet, bare	7.3 ± 0.04	33.2 ± 1.08	8.2 ± 0.71	31.2 ± 0.96	10.4 ± 0.85	31.5 ± 0.37	10.3 ± 0.38	19.2 ± 3.45
Dry, bare	7.7 ± 0.37	5.2 ± 1.37	6.5 ± 0.12	13.1 ± 0.80	6.1 ± 0.12	11.8 ± 0.60	7.1 ± 0.13	11.0 ± 1.80
Dry, 1.5 cm litter	4.2 ± 0.13	6.8 ± 0.24	5.4 ± 0.02	11.1 ± 0.25	6.0 ± 0.05	12.0 ± 0.73	7.2 ± 0.39	12.7 ± 1.74
NIMS, 5 m location, 4.2 cm litter	3.1 ± 0.08	4.9 ± 0.78	5.5 ± 0.07	12.6 ± 1.26	7.4 ± 0.13	12.1 ± 1.27	7.0 ± 0.30	11.8 ± 1.67
NIMS, 7 m location, 6.7 cm litter	3.3 ± 0.34	6.1 ± 0.13	5.1 ± 1.02	11.0 ± 1.38	6.6 ± 0.09	14.1 ± 1.34	8.9 ± 0.14	10.1 ± 0.41

(10.3° view angle) on March 18, 2007 and at the widest view angle (41.3°) on August 12, 2007. Images were collected continuously in a slightly overlapping circular pattern in order to create a time series of panoramas of the entire forest gap for each day. The time between complete panoramas was 30 min for March and 10 min for August. Panoramas were then compared to an initial panorama created in the mornings of the same days, when no sunflecks occurred in the forest gap, to establish areas of different soil surface reflectivity; these early panoramas were subsequently subtracted from later ones and the results thresholded at 50% of the maximum value into binary images using a program written in Python with the Python Imaging Library (Secret Labs AB; Linköping, Sweden; www.pythonware.com) set of tools. Panoramas for March were scaled to those collected in August and then each was examined in 3 × 3 blocks of pixels for sunfleck analysis. The total number of blocks examined was 199,544 covering 644.9 m^2 of forest gap soil surface. The total area per block of pixels was established from an exponential calibration of distance related to camera tilt using a meter stick and repeated photographs.

2.4. Models

A modified sinusoidal model was based on a simpler model that uses a single "damping depth", the depth at which the amplitude of the temperature variation is attenuated to 37% of that at the surface, to also describe the accompanying phase shift with depth (Van Wijk and de Vries, 1966). The single damping depth was divided into both attenuation (decrease in amplitude) and delay (phase shift) depths in the modified sinusoidal model and fit to multiple-day measurements in the four NIMS transect locations during the two dates of measurement using a least squares optimization in R, a freely available language and environment for statistical computing and graphics (R Development Core Team, 2006; www.cran.r-project.org). The modified sinusoidal model is thus:

$$T_z = \bar{T}^{surf} + \Delta T^{surf} e^{-z/d_1} \cos\left(\frac{2\pi t}{p} - \frac{2\pi t_{max}}{p} - \frac{z}{d_2}\right) \quad (1)$$

where T_z is the temperature at any depth z in the soil, $\bar{T}^{surf}$ is the average surface temperature, ΔT^{surf} is the amplitude of temperature variation at the surface, d_1 is the attenuation depth, t_{max} is the time at which the surface is at the maximum temperature, and d_2 is the delay depth describing the time for the temperature maximum to be reached at depth z.

Fourier transforms (FT) of the uneven but periodic temperature oscillations at the surface and at depth were used with Eq. (1) to estimate d_1 and d_2 for different harmonic periods. Specifically, after the FT decomposition of the surface temperature signal, the multiple constituent surface temperature sine waves of different harmonic periods were transformed by the modified sinusoidal model and then summed to calculate the 2, 8, and 16 cm subsurface temperatures. Values for d_1 and d_2 were optimized with measured data at 2, 8, and 16 cm depths and then averaged and used to predict subsurface temperatures in different surface locations.

A time series of direct solar radiation for the entire forest gap in each thresholded panoramic image was established for each pixel by the average value of the surrounding eight binary pixels in the image. Pixels that included vegetation that masked the soil surface from the view of the camera were removed from analysis. Averaged pixel values then ranged from 0.0 to 1.0 and were related to soil surface temperature using an empirical model (Eq. (2)) based on the combination of two general methods used to predict soil temperature or heat flux used in remote sensing, one relating net solar radiation to soil heat flux (e.g., Santanello and Friedl, 2003) and the other equating air temperature to soil surface temperature (e.g., Bond-Lamberty et al., 2005):

$$T_t^{est} = \text{pixel value} \times T_{max}^{surf}$$
$$\text{if } T_t^{est} < T_t^{air} : T_t^{est} = T_t^{air} \quad (2)$$

where T_t^{est} is the estimated temperature of the soil surface at time t for any given pixel, T_{max}^{surf} is the maximum observed temperature of the soil surface during a 24 h period, and T_t^{air} is the observed air temperature at time t. The procedure was as follows: each pixel in the image was assigned a soil temperature equal to the averaged pixel value multiplied by the maximum observed soil surface temperature. After this assignment, if the soil surface temperature for any pixel was below that of the air temperature for the time period, then the soil surface temperature was assigned the value of the air temperature. Each pixel in the 24 h sequence of images represented a separate temperature time series that was then treated with the same FT decomposition and reconstruction of subsurface temperatures as above, using the previously determined d_1 and d_2 values for the forest gap on each of the separate dates of measurement.

3. Results

Different locations of soil surface in the forest understory received different repeated but uneven patterns of solar input (Fig. 1). Such different surface temperature patterns were also evident in the subsurface soil but with attenuated and delayed temperature peaks, which depended on soil conditions. For example, the peak soil temperature at the surface for a dried soil occurred at 13:26 h and for an untreated site at a distance of 3 m away, the peak occurred 1.5 h later (Fig. 1A and C). The condition of the soil (wet or dry) also affected the time of day at which the temperature was at its maximum at various depths. For two locations within 1 m of each other, one dried and the other maintained with a moisture content near field capacity, the temperature peak at 8 cm depth occurred 2.7 h later than at the surface for the dry soil and 0.9 h later for the wet soil (Fig. 1A and B). Soil water content also altered d_1 of the daily temperature variation. For example, the difference in maximum temperature between the surface and at 8 cm depth for a dried soil was 37.8 °C and for a wet soil was 21.9 °C. High-frequency changes in the surface temperature of the soil were conducted into the soil proportionally less than low-frequency changes for both wet and dry soils (Fig. 1).
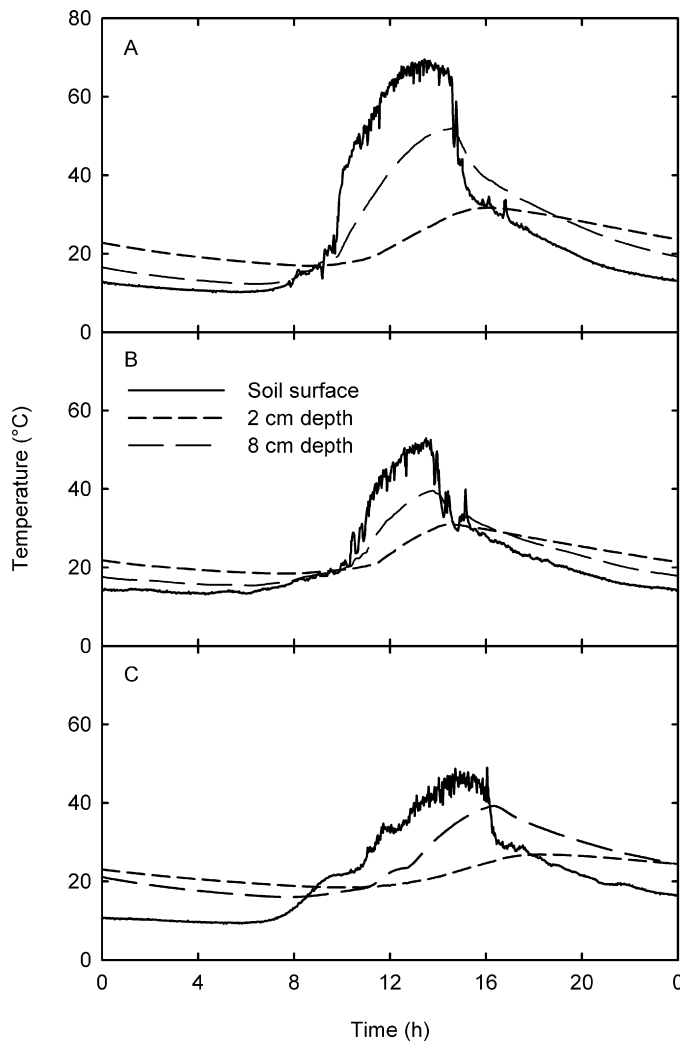
Fig. 1. Measured soil temperatures for 24 h at the mineral soil surface (solid line) under a thin layer of leaf litter, at 2 cm depth (long dash), and at 8 cm depth (short dash) for (A) a dried, partly shaded location, (B) a wetted, partly shaded location, and (C) an untreated, mostly shaded location. Data for all three locations were collected on similarly sunny days within the first week in July of 2007 and all locations are within a radius of 3 m from each other.

Fig. 2. Measured soil temperature for the same location in Fig. 1A (solid gray line) and FT reconstructions of soil temperature for the largest, first harmonic component (24 h; dotted lines), the sum of the first and second components (24 and 12 h; short dashed line), and the sum of the first eight components (24–3 h; solid line) at (A) the surface, (B) at 2 cm depth, and (C) at 8 cm depth.

Both d_1 and d_2 varied with distance between soil layers and with conditions of the soil (Table 1). Both d_1 and d_2 were greater for wet soils than for dry, except for when calculating d_1 between shallow layers (surface to 2 cm depth). d_2 tended to be larger than d_1, except for the shallow layer case in a dry soil. A thin mostly pine needle leaf litter did not seem to greatly affect d_1 or d_2. Both d_1 and d_2 were similar when calculated for the soil layers 0–8 cm and for 2–8 cm (Table 1).

Daily surface and subsurface soil temperature cycles at different locations in the forest understory were reconstructed with increasing accuracy using an increasing number of component harmonic sine waves derived from a FT of the original signal (Fig. 2). Apart from a constant offset, the largest FT harmonic component of the daily signal at upto 8 cm depth was the 24 h temperature signal. The single 24 h sine wave function was not a good predictor of the actual temperature at the surface (RMSE is 8.2 °C), although it became a better predictor at greater depths (Fig. 2B and C). The addition of the second largest harmonic component of the signal, with a period of 12 h, increased the accuracy of temperature reconstruction at the surface of a dried soil to an RMSE of 4.6 °C. Using the first eight harmonic components to reconstruct the surface temperature resulted in an RMSE of 1.3 °C. In comparison, the RMSE
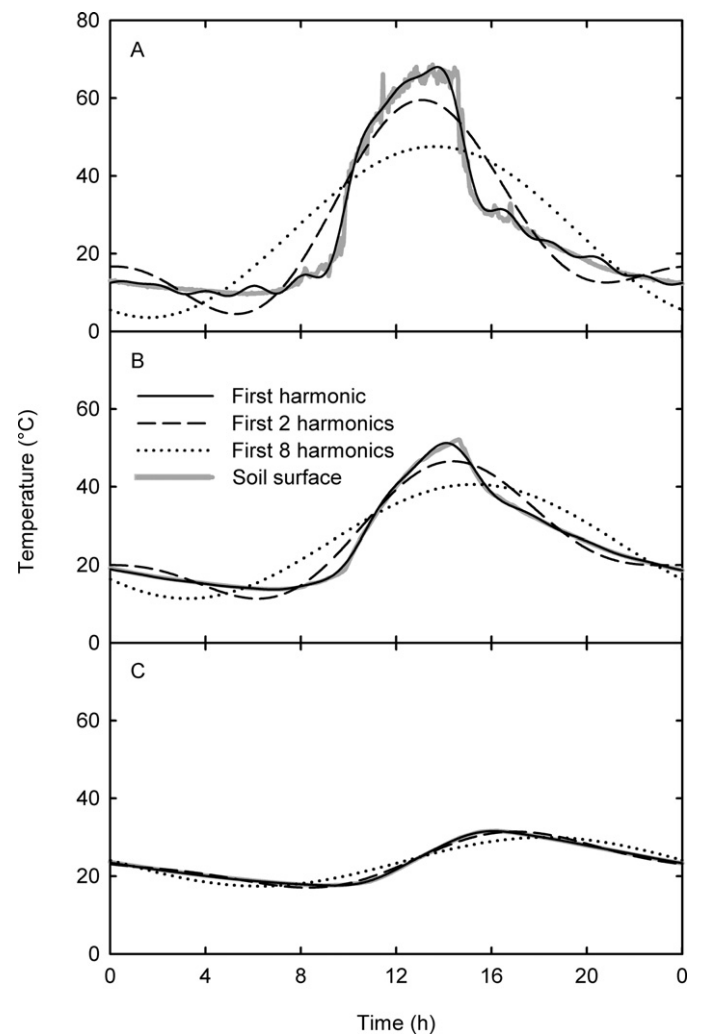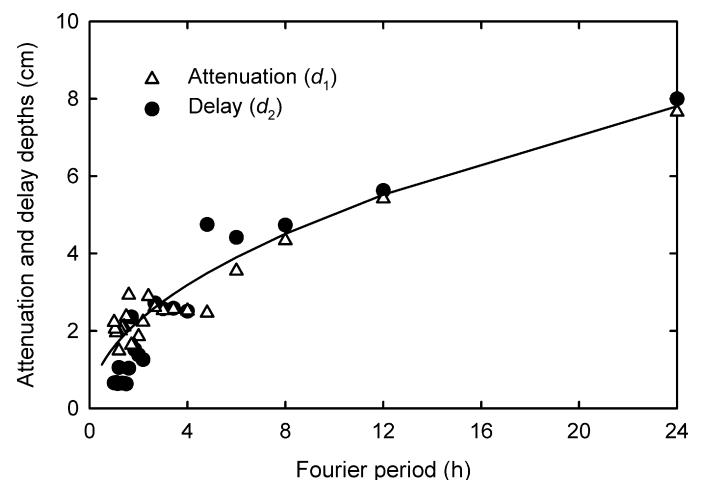

Fig. 3. Attenuation (open triangle) and delay (closed circle) depths calculated for each harmonic component of an FT decomposition for 24 h of surface temperatures of a dry soil. The theoretical "damping depth" calculated from thermal properties of the soil is indicated with a solid line.

Table 2
Root mean square errors and maximum difference between calculated and measured values of temperatures over 24 h for unmodified and modified sinusoidal models using Fourier analysis predicting subsurface temperatures from surface layers of a dry soil; values were sampled at about 72 s intervals for 24 h.

	Fourier components (shortest period)	RMS error (°C)				Maximum absolute difference (°C)			
		0–2 cm	0–8 cm	2–8 cm	8–16 cm	0–2 cm	0–8 cm	2–8 cm	8–16 cm
Simple model	One frequency (24 h)	5.62	1.76	1.67	0.40	13.35	4.09	3.38	0.84
	Four frequencies (6 h)	0.95	0.62	0.24	0.18	4.25	1.17	0.67	0.37
	Eight frequencies (3 h)	0.59	0.62	0.23	0.18	2.23	1.09	0.57	0.38
Modified model	One frequency (24 h)	5.61	1.66	1.66	0.34	13.07	3.25	3.14	0.84
	Four frequencies (6 h)	0.90	0.08	0.14	0.18	4.28	0.25	0.30	0.35
	Eight frequencies (3 h)	0.49	0.04	0.12	0.18	2.58	0.15	0.24	0.38

of reconstruction of temperature at 8 cm using only the first 24 h period was 1.7 °C and using the first eight harmonic components was 0.1 °C (Fig. 2C). Artifacts of the technique are apparent at the surface when using only eight harmonic components, with higher frequency oscillations (about 2 h in period) occurring within the original signal (Fig. 2A).

The unmodified and modified sinusoidal temperature models were compared to predict deeper layer temperatures using different numbers of harmonic components of the FT of overlying soil layers (Table 2). Predictions of subsurface temperatures using only the largest harmonic component from the FT resulted in sim-

ilar errors and maximum differences between models and adding FT harmonic components increased accuracy in both. Predicting temperatures between shallow layers (surface to 2 cm depth) resulted in the greatest errors and maximum differences compared to predicting temperatures between more separated depths. The modified sinusoidal model predicted subsurface temperatures more accurately between separated layers of soil than the unmodified model when more than one harmonic component was used (Table 2).

Both d_1 and d_2 for a dry soil decreased with decreasing FT harmonic components (Fig. 3). Such decreases were similar between d_1
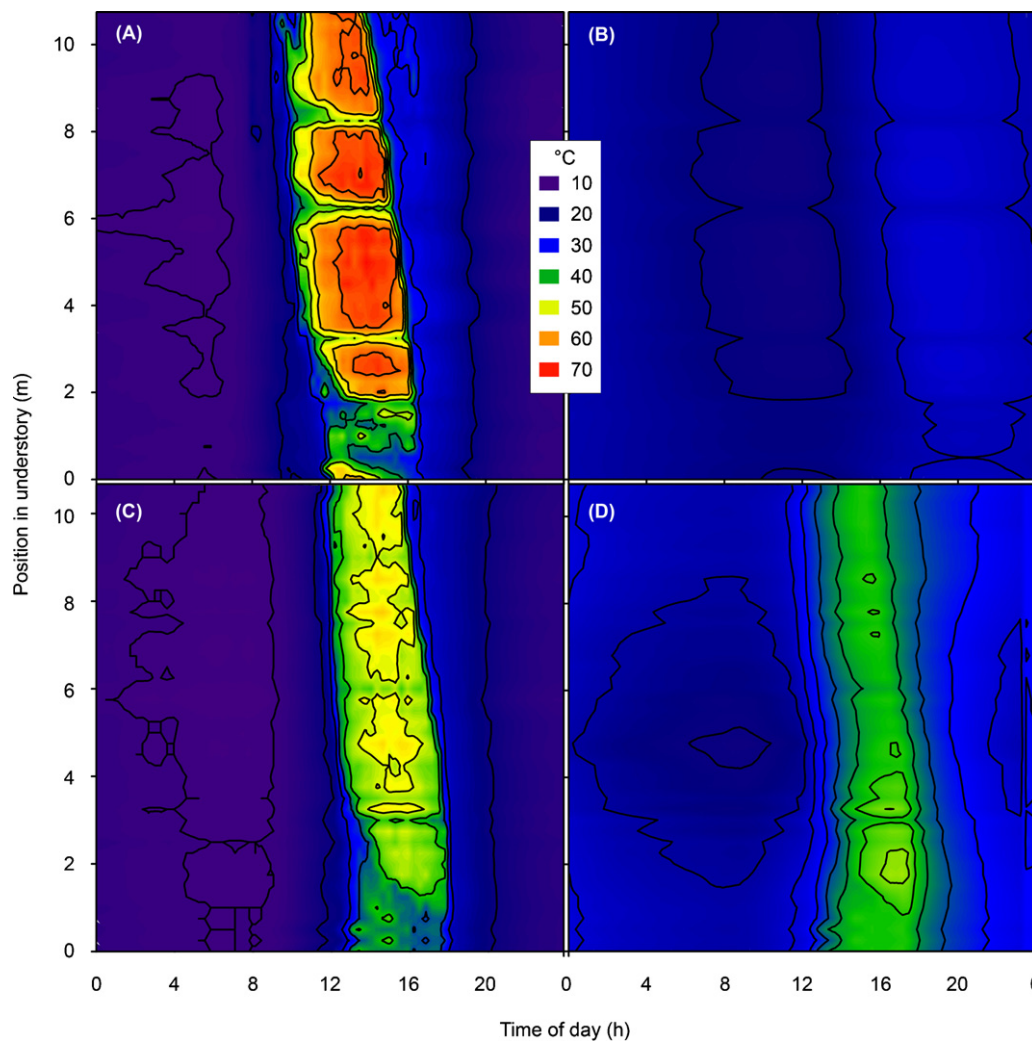

Fig. 4. Soil temperature data for 24 h along a 10.75 m transect on (A and B) July 16, 2007 and on (C and D) March 3, 2008. Soil temperatures at (A and C) the surface were measured every 0.25 m and those at (B and D) 8 cm depth were calculated using the modified sinusoidal model and FT.

and d_2 and followed the theoretical trend based on heat conduction models for homogeneous solids. The concordance with the theoretical and measured d_1 and d_2 indicated that using the theoretical value based on soil physical properties as an initial parameter for calculating best fits for both d_1 and d_2 was appropriate. The maximum absolute difference between the theoretical and measured d_1 was 0.15 cm and for d_2 was 0.19 cm.

Soil surface temperature measured over a 24 h period in July 2007 with the mobile NIMS resulted in a maximum measured temperature of 77.5 °C and a minimum of 8.7 °C (Fig. 4A) with an average of 26.7 ± 21.8 °C (mean ± SD). Time of day varied for the maximum temperature along the NIMS transect. For example, the maximum temperature at the 3 m position along the NIMS transect occurred at 13:36 h and at the 10 m position occurred 18.4 min later. Surface temperatures were affected by shadows of the overlying vegetation and were not strongly correlated with leaf litter thickness (data not shown). The predicted temperature at 8 cm depth was maximal at about 5 h after the maximal at the surface (Fig. 4B). The maximum temperature at 8 cm depth was 28.1 °C and the minimum was 17.7 °C. At the 1 m position on the NIMS transect where overlying vegetation was most dense and shading greatly altered the pattern of soil surface heating, the minimum temperature was about 2.6 °C warmer than at 3 m farther into the transect where shading was less.

The NIMS transect was measured again in early March of 2008, after the soil had been wetted by winter rains. The maximum surface temperature was 57.4 °C and the minimum was −2.1 °C (Fig. 4C), about 87% of the temperature range measured in July. The average temperature in March at 4 m along the NIMS transect was 13.3 ± 17.8 °C, about 14.0 ± 9.4 °C cooler than in July. The maximum temperature at 3 m along the transect occurred about 2.3 h later than in July. The predicted temperature at 8 cm depth was maximal 1.9 h after the maximum at the surface (Fig. 4D) at 46.8 °C with the minimum of 9.3 °C. At the 1 m position on the transect, the minimum temperature achieved was about 3.2 °C warmer than at 3 m farther into the transect where shading was less.

Simultaneous measurements of air temperature, soil surface temperature, and incident shortwave radiation at four locations under the NIMS transect were used to create the sunfleck model (Eq. (2)) for soil surface temperature as a function of air temperature, maximum 24-h surface temperature, and timing of direct sunlight. Measured soil surface temperatures were similar to air temperatures during times of the day without incident direct sunlight for all locations (Fig. 5A and B). A sharp rise in soil surface temperature above that of air temperature occurred with incident direct sunlight and modeled soil surface temperature captured this trend (Fig. 5B). Subsurface temperature estimations, based on the surface temperature model and the modified sinusoidal model, were also similar to those measured (Fig. 5C), deviating by only a few degrees.

Panoramic composite images of the forest gap soil captured with the PTZ digital camera captured the dynamic light environment of the soil surface (Fig. 6). Single images within the composite varied in average pixel intensity (Fig. 6A and B) because of automatic exposure compensation by the camera and different reflectivity of the soil surface in portions of the forest gap. These differences were removed after subtracting images taken from the same pan-tilt camera location but captured before direct sunlight was present. Subsequent thresholding of each image within the panorama created binary (black and white) images that captured shadowed and sunlit portions of the soil surface for multiple time periods (Fig. 6C and D).

The percentage of soil surface area in the forest gap receiving direct sunlight as measured with the digital camera differed between the two dates measured (Fig. 7). The maximum amount of time that any one pixel's amount of soil surface area received direct sunlight was 6.5 h in March and 9.5 h in July. The average
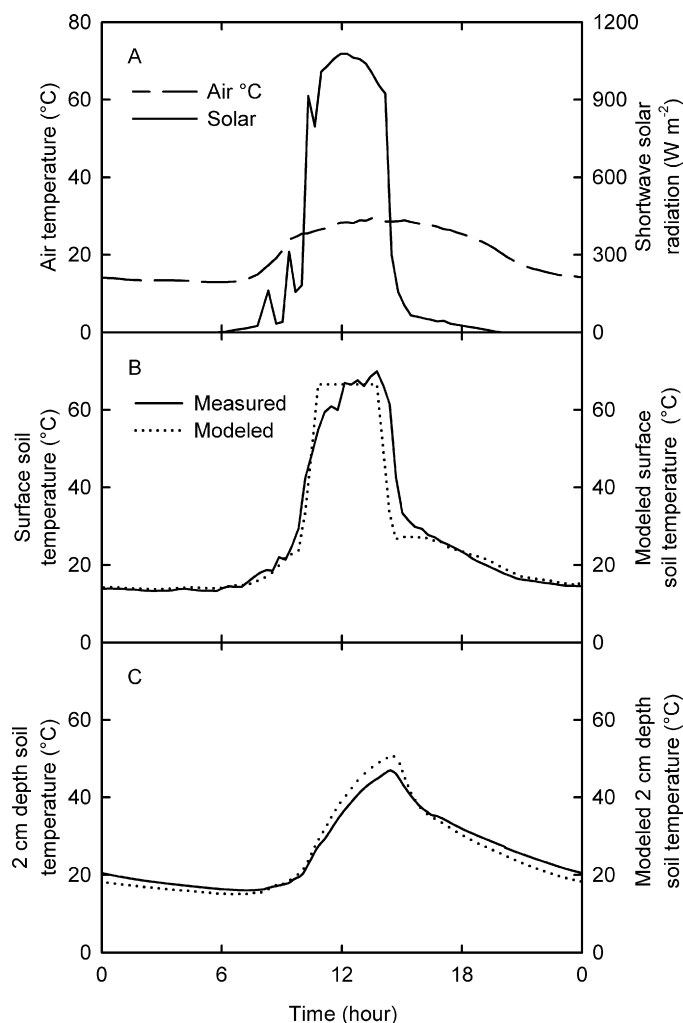

Fig. 5. Representative 24 h time series of (A) air temperature (long dash) and shortwave solar radiation (solid line), (B) measured (solid line) and modeled (dotted line) soil surface temperature, and (C) measured and modeled soil temperature at 2 cm depth along the NIMS transect on July 15, 2007.

amount of time that each pixel received direct sunlight, not including those that received none, was 3.1 h in March and 3.3 h in July. The most frequently occurring amount of time for any pixel to be in direct sunlight was 4 h in March and 3.5 h in July (Fig. 7).

The spatial distribution of the amount of time that any pixel in the panoramas of the forest gap received direct sunlight varied between the two dates of measurements (Fig. 8). For example, the areas that were farthest from the camera in the forest gap (Fig. 8A, top of the image) received the greatest amount of direct sunlight over the course of the day in both March and July (Fig. 8B). Different areas in the forest gap in July received additional direct sunlight, based on the difference values between July and March (Fig. 8B, lower left of the image). Only small amounts of area in July received less direct sunlight than in March (data not shown).

Using the surface temperature calculations based on received direct sunlight as detected with the camera, measured air temperature, and the first 20 harmonic components from a FT of this temperature series, subsurface temperature to 8 cm depth was calculated for each pixel based on previously determined values of d_1 and d_2 using the modified sinusoidal model. In March, the maximum positive change in temperature of a unit volume of soil, as defined by a single pixel, was 1.5 °C during 30 min and the negative change was 1.3 °C. In July, the maximum positive change was 1.8 °C and negative change was 1.6 °C. In March when the soil was
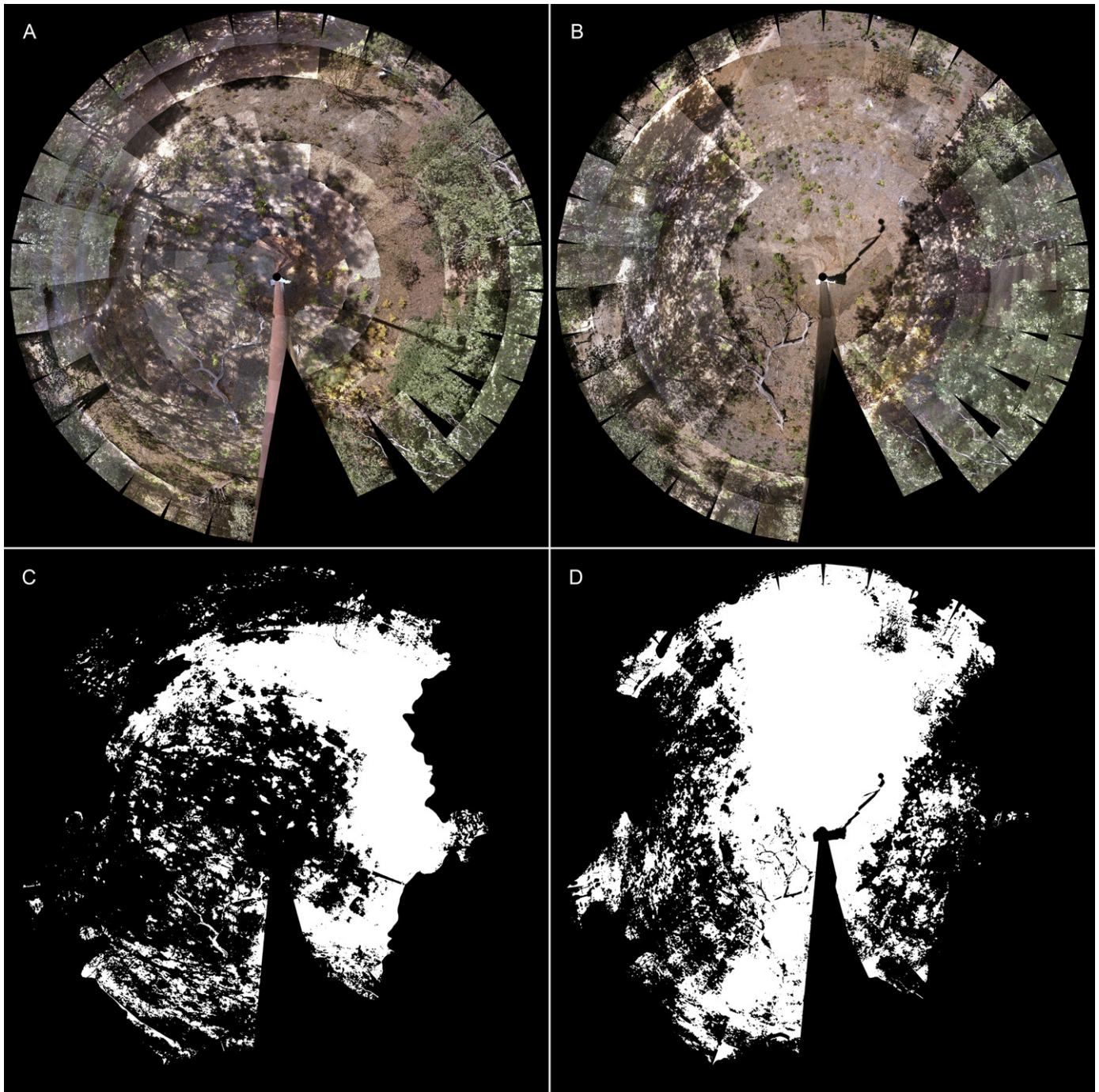
Fig. 6. Representative panoramic images of a forest gap constructed from multiple 640 × 480 pixel images captured with a pan-tilt-zoom camera positioned at the top of a 10 m tower at the James Reserve in July of 2007. The NIMS supporting cables and sensor platform is located in the upper right of the composite image. Panoramas were captured at (A) 10:10 h and (B) 11:40 h. Images captured at 07:20 h were subtracted from subsequent images and the resulting difference image was thresholded to result in (C and D) binary images for each time period. Vegetation is masked as black after thresholding.

wet, the maximum surface heat flux was 0.21 kJ m^{-2} s^{-1}. In July, the maximum surface heat flux was 0.29 kJ m^{-2} s^{-1}. The heat balance for both dates for a 24 h period, as calculated by this method, was effectively zero. The total heat stored and then lost over the course of a day was 2.49 GJ d^{-1} for the 645 m^2 area of forest gap in March and 3.36 GJ d^{-1} in July.

4. Discussion

The soil surface and subsurface in a forested environment can be influenced by canopy shading, causing uneven but periodic changes in temperature that deviate from the simple sinusoidal models that are often used to predict soil temperature and energy balance. Yet estimates of hourly energy budgets used for eddy flux measurements usually depend on a very limited number of fixed-locations for measurement of spatially and temporally heterogeneous of soil heat fluxes (e.g., Ogée et al., 2001). The spatial variability of leaf area index makes even evapotranspiration impractical to model over heterogeneous lands (Suleiman and Crago, 2004). This limitation is important to consider in both studies of forest soil CO_2 efflux, with the greatest temporal variations of temperature occurring near the soil surface, as well as those of plant distribution,
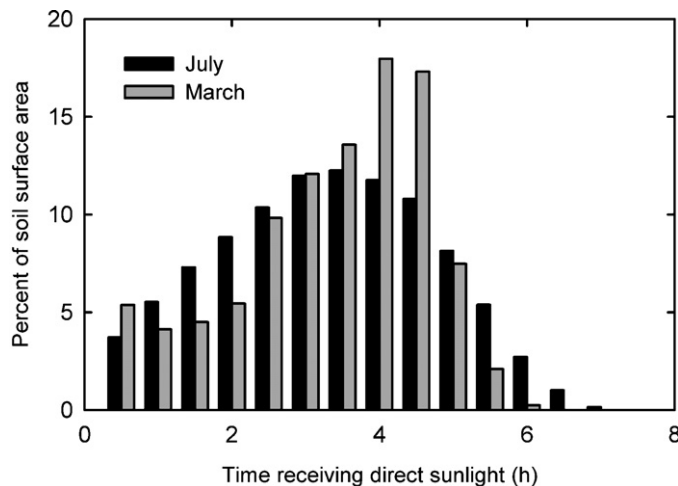
Fig. 7. Percentage of soil surface area in the forest gap over 24 h with direct incident solar radiation, as determined from repeated thresholded panoramic images. Areas of vegetation and soil surface that did not receive direct solar radiation were ignored. Measurements made in March are indicated by solid grey bars and those made in July by solid black bars.

where forest gaps and their associated microclimates are thought to play a major role in the regeneration of many plant species in both tropical and temperate areas (Balisky and Burton, 1995; Schnitzer et al., 2000).

Sinusoidal models for heat conduction in soil historically have been used (Van Wijk and de Vries, 1966) and continue to be used (Chen et al., 2009) because of their simplicity and first-principles derivation. The use of the same value for both attenuation of the surface temperature oscillation and the delay of the maximum with depth in these equations is based on a uniformly conducting solid. Introducing two variables for this one parameter adds an increased in accuracy for predicting subsurface temperatures from surface temperatures but at the cost of some physically based explanations of how heat conduction is occurring. We also acknowledge that this modified sinusoidal model also adds yet one more variation on the plethora of variations that exist for this simple and powerful model that is by itself sufficient for many agricultural and exposed location applications.

Longer time-scale variations of soil temperatures are caused by a juxtaposition of local weather conditions and seasonal variations and can create even more complex signals. Indeed, we observed such longer time-scale changes in subsurface temperatures and chose relatively similar days in order to test our methodology. However, using FT, all signals can be modeled using a series of superimposed sine waves and superimposing annual and daily surface temperature sinusoids achieves more accuracy in predicting heat flux in soil (Hu et al., 2002; Elias et al., 2004; Droulia et al., 2009). The method for applying a sine wave soil heat conduction model to each of the harmonic components of a FT decomposition has long been recognized to improve accuracy of predicting subsurface temperatures (Van Wijk and de Vries, 1966; Ballard, 1972). Modern computing power and relatively simple programming languages like Python have allowed us to not only easily compute the FT of a complex signal but to apply a model to every resultant harmonic and then recombine them rapidly.

Mobility of sensor platforms is accompanied by many challenges, including optimizing the spatiotemporal components of sampling; however the ability to rapidly deploy the cabled system and automatically and adaptively relocate sensing equipment has proved to significantly increase sensing system performance (Rahimi et al., 2005). Several studies have incorporated mobility with environmental sensing, decreasing sensing uncertainty and
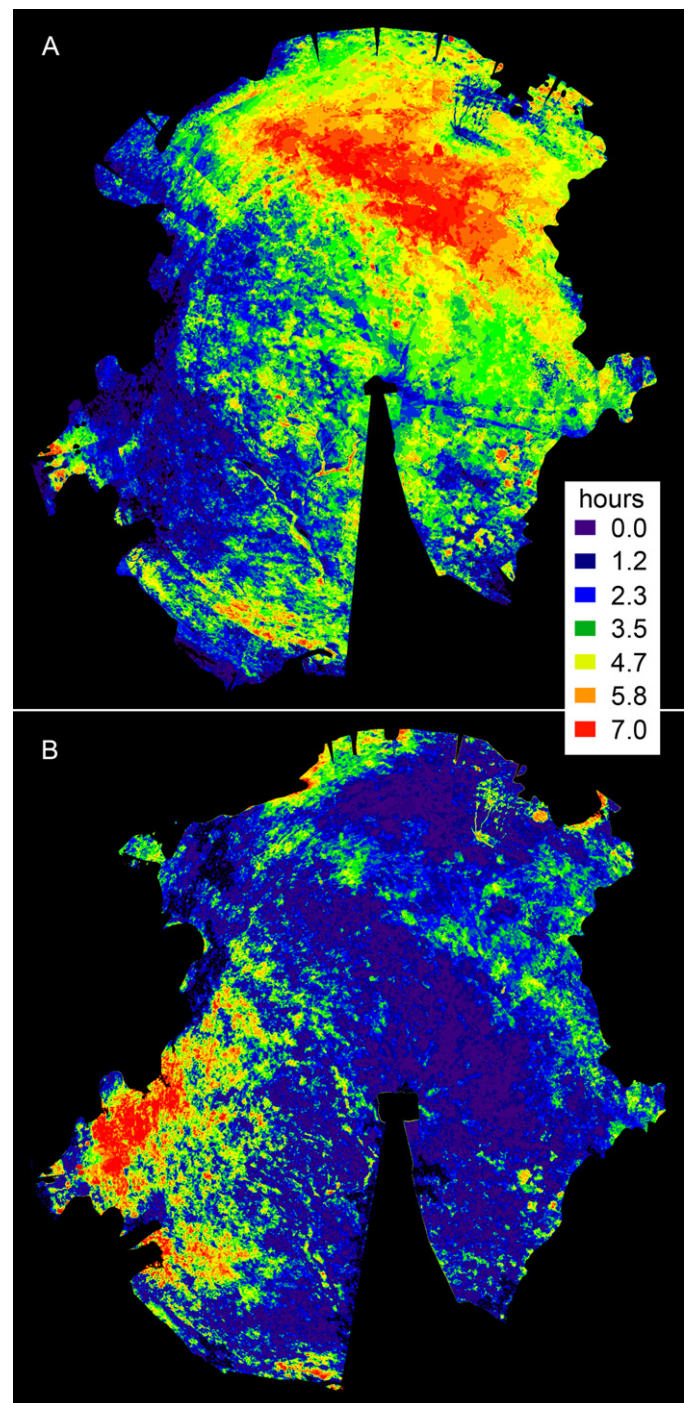

Fig. 8. Spatial representation of the total amount of time that each corresponding pixel in a daily time series of panoramic images received direct solar radiation for (A) March, and (B) the time difference between March and July. Negative values, indicating less direct solar radiation per pixel in July than in March in panel (B) are not shown.

increasing the physical range of sensing (Caron et al., 2008; Graham et al., 2009) or time of sampling (Singh et al., 2007). Innovation in movement of sensors in three dimensions promises even greater sensing capabilities (Borgstrom et al., 2007). In this study, mobility of sensors along a linear transect allowed us to measure soil surface temperature at a high spatial resolution over the course of multiple days while simultaneously sampling with fixed sensors.

Visible light digital cameras are increasingly being used in environmental sensing (Hamilton et al., 2007; Morisette et al., 2009;

Porter et al., 2009). Automatic image segmentation by thresholding is a commonly used image processing technique in ecological applications (Cescatti, 2007; Graham et al., 2009). Simple image processing techniques are making standard the use of digital cameras for the detection of plant phenological events (Crimmins and Crimmins, 2008; Graham et al., 2009, in press; Morisette et al., 2009; Richardson et al., 2009) as well as for automating a range of agricultural monitoring practices (Jia et al., 2004; Slaughter et al., 2008). The uses of cameras in these studies have been primarily based on the color reflectance of plants. Although many studies have used visible light cameras to determine canopy structure and estimate the effect of sunflecks using upwardly facing hemispherical lenses (e.g., Jonckheere et al., 2004), to the best of our knowledge this study appears to be the first to use a camera to examine the resultant spatial and temporal patterns of reflected solar radiation on a forest soil surface. We have demonstrated that the combination of digital imagery, the Fourier transform decomposition of these complex signals, and heat conduction models can be applied to expand single-location measurements of temperature and heat balance to larger areas that are heterogeneous in both time and space.

Although we only tested the use of a camera and the combination of temperature models in one location for predicting soil surface and subsurface temperature, the application of this method to other locations should be straight-forward. Our use of a mobile sensor platform allowed us to test our heat conduction model along a transect but this is not necessary for application to other locations. Our method was an empirical one, predicting soil surface and subsurface temperature using measured maximum surface temperature (which would be affected by both soil properties in different locations and solar conditions during different times of the year), measured subsurface temperature, air temperature, and visibly reflected sunflecks. Limitations to our method may include errors associated with canopy vegetation differentially insulating soil from radiation loss at night, insulation from snow, a deep leaf litter layer, or other soil surface energy balance factors that would require more complicated modeling.

Much work has been done on algorithms to integrate sensor data collected at different times and from multiple observation platforms (e.g., Mysorewala et al., 2009). Hierarchical systems that enable the autonomous arrangement of sensors can optimize sensing fidelity and spatial coverage and have resulted in algorithms to increase the fidelity sampling of high-frequency spatiotemporal environmental phenomena (Singh et al., 2006). In this study, we were able to coordinate a higher level sensor, the digital camera, as a top-tier but lower resolution sensor with in situ, higher resolution sensors, creating a multiscale sensing system for soil surface and subsurface temperature measurement. Including multiple sensing tiers from buried and surface sensors with a digital camera appears a practical and efficient method for measuring wide area temperatures and heat fluxes in temporally and spatially heterogeneous environments.

Acknowledgements

References

Balisky, A.C., Burton, P.J., 1995. Root-zone soil temperature variation associated with microsite characteristics in high-elevation forest openings in the interior of British Columbia. Agric. For. Meteorol. 77, 31–54.

Ballard, T.M., 1972. Subalpine soil temperature regimes in southwestern British Columbia. Arct. Alp. Res. 4, 139–146.

Bond-Lamberty, B., Wang, C., Gower, S.T., 2005. Spatiotemporal measurement and modeling of stand-level boreal forest soil temperatures. Agric. For. Meteorol. 131, 27–40.

Borgstrom, P.H., Borgstrom, N.P., Stealey, M.J., Jordan, B., Sukhatme, G., Batalin, M.A., Kaiser, W.J., 2007. Discrete trajectory control algorithms for NIMS3D, an autonomous underconstrained three-dimensional cabled robot. In: Proceedings of the 2007 IEEE/RSJ International Conference on Intelligent Robots and Systems, San Diego, CA, USA, pp. 253–260.

Caron, D.A., Stauffer, B., Moorthi, S., Singh, A., Batalin, M., Graham, E.A., Hansen, M., Kaiser, W.J., Das, J., Pereira, A., Dhariwal, A., Zhang, B., Oberg, C., Sukhatme, G.S., 2008. Macro- to fine-scale spatial and temporal distributions and dynamics of phytoplankton and their environmental driving forces in a small montane lake in southern California, USA. Limnol. Oceanogr. 53, 2333–2349.

Cescatti, A., 2007. Indirect estimates of canopy gap fraction based on the linear conversion of hemispherical photographs, Methodology and comparison with standard thresholding techniques. Agric. For. Meteorol. 143, 1–12.

Chang, K., Yau, N., Hansen, M.H., Estrin, D., 2006. SensorBase.org—a centralized repository to slog sensor network data. Proceedings of the International Conference on Distributed Networks (DCOSS)/EAWMS.

Chen, J.M., Huang, S.E., Ju, W., Gaumont-Guay, D., Black, T.A., 2009. Daily heterotrophic respiration model considering the diurnal temperature variability in the soil. J. Geophys. Res. (G Biogeosci.) 114, G01022.

Crimmins, M.A., Crimmins, T.M., 2008. Monitoring plant phenology using digital repeat photography. Environ. Manage. 41, 949–958.

Droulia, F., Lykoudis, S., Tsiros, I., Alvertos, N., Akylas, E., Garofalakis, I., 2009. Ground temperature estimations using simplified analytical and semi-empirical approaches. Solar Energy 83, 211–219.

Elias, E.A., Cichota, R., Torriani, H.H., van Lier, Q.D.J., 2004. Analytical soil-temperature model, correction for temporal variation of daily amplitude. Soil Sci. Soc. Am. J. 68, 784–788.

Gaumont-Guay, D., Black, T.A., McCaughey, H., Barr, A.G., Krishnan, P., Jassal, R.S., Nesic, Z., 2009. Soil CO_2 efflux in contrasting boreal deciduous and coniferous stands and its contribution to the ecosystem carbon balance. Global Change Biol. 15, 1302–1319.

Geiger, R., Aron, R.H., Todhunter, P., 2003. The Climate Near the Ground, 6th ed. Rowman & Littlefield Publishers, Inc., New York, p. 584.

Gonzalez-Dugo, M.P., Neale, C.M.U., Mateos, L., Kustas, W.P., Prueger, J.H., Anderson, M.C., Li, F., 2009. A comparison of operational remote sensing-based models for estimating crop evapotranspiration. Agric. For. Meteorol. 149, 1843–1853.

Graham, E.A., Yuen, E.M., Robertson, G.F., Kaiser, W.J., Hamilton, M.P., Rundel, P.W., 2009. Budburst and leaf area expansion measured with a novel mobile camera system and simple color thresholding. Environ. Exp. Bot. 65, 238–244.

E.A. Graham, E.C. Riordan, E.M. Yuen, D. Estrin, P.W. Rundel. Public internet-connected cameras used as a cross-continental ground-based plant phenology monitoring system. Global Change Biology, in press.

Hamilton, M.P., Rundel, P.W., Allen, M.F.A., Kaiser, W., Hansen, M.H., Estrin, D.L.E., Graham, E.A., 2007. New approaches in embedded networked sensing for terrestrial ecological observatories. Environ. Eng. Sci. 24, 192–204.

Hardy, J.P., Melloh, R., Koenig, G., Marks, D., Winstral, A., Pomeroy, J.W., Link, T., 2004. Solar radiation transmission through conifer canopies. Agric. For. Meteorol. 126, 257–270.

Harmon, T.C., Ambrose, R.F., Gilbert, R.M., Fisher, J.C., Stealey, M., Kaiser, W.J., 2007. High-resolution river hydraulic and water quality characterization using rapidly deployable networked infomechanical systems (NIMS RD). Environ. Eng. Sci. 24, 151–159.

Hu, Q., Feng, S., Schaefer, G., 2002. Quality control for USDA NRCS SM-ST network soil temperatures, a method and a dataset. J. Appl. Meteorol. 41, 607–619.

Ishida, M., 2004. Automatic thresholding for digital hemispherical photography. Can. J. For. Res.: Rev. Can. Rech. For. 34, 2208–2216.

Jia, L., Chen, X., Zhang, F., Buerkert, A., Roemheld, V., 2004. Use of digital camera to assess nitrogen status of winter wheat in the northern China plain. J. Plant Nutr. 27, 441–450.

Jordan, B.L., Batalin, M.A., Kaiser, W.J., 2007. NIMS RD: a rapidly deployable cable based robot. In: IEEE International Conference on Robotics and Automation, Rome, Italy, pp. 144–150.

Jonckheere, I., Fleck, A., Nackaerts, K., Muys, B., Coppin, P., Weiss, M., Baret, F., 2004. Review of methods for in situ leaf area index determination, part I. Theories, sensors and hemispherical photography. Agric. For. Meteorol. 121, 19–35.

Körner, C., Paulsen, J., 2004. A world-wide study of high altitude treeline temperatures. J. Biogeogr. 31, 713–732.

Morisette, J.T., Richardson, A.D., Knapp, A.K., Graham, E.A., Abatzoglou, J., Wilson, B.E., Breshears, D.D., Henebry, G., Hanes, J.M., Lang, L., 2009. Tracking the rhythm of the seasons in the face of global change: phenological research in the 21st century. Front. Ecol. Environ. 7, 253–260.

Mysorewala, M.F., Popa, D.O., Lewis, F.L., 2009. Multi-scale adaptive sampling with mobile agents for mapping of forest fires. J. Intell. Robotic Syst. 54, 535–565.

Nusier, O.K., Abu-Hamdeh, N.H., 2003. Laboratory techniques to evaluate thermal conductivity for some soils. Heat Mass Transfer 39, 119–123.

Ogée, J., Lamaud, E., Brunet, Y., Berbigier, P., Bonnefond, J.M., 2001. A long-term study of soil heat flux under a forest canopy. Agric. For. Meteorol. 106, 173–186.

Paul, K.I., Polglase, P.J., Smethrust, P.J., O'Connell, A.M., Carlyle, C.J., Khanna, P.K., 2004. Soil temperature under forests: a simple model for predicting soil temperature under a range of forest types. Agric. For. Meteorol. 121, 167–182.

Porter, J.H., Nagy, E., Kratz, T.K., Hanson, P., Collins, S.L., Arzberger, P., 2009. New eyes on the world: advanced sensors for ecology. Bioscience 59, 385–397.

Qiu, G.Y., Yano, T., Momii, K., 1998. An improved methodology to measure evaporation from bare soil based on comparison of surface temperature with a dry soil surface. J. Hydrol. 210, 93–105.

R Development Core Team, 2006. R: a language and environment for statistical computing. R Foundation for Statistical Computing, Vienna, Austria. ISBN 3-900051-07-0, URL: http://www.R-project.org.

Rahimi, M., Hansen, M.H., Kaiser, W.J., Sukhatme, G.S., Estrin, D., 2005. Adaptive sampling for environmental field estimation using robotic sensors. In: Proceedings IEEE/RSJ International Conference on Intelligent Robots and Systems (IROS), pp. 3692–3698.

Richardson, A.D., Braswell, B.H., Hollinger, D.Y., Jenkins, J.P., Ollinger, S.V., 2009. Near-surface remote sensing of spatial and temporal variation in canopy phenology. Ecol. Appl. 19, 1417–1428.

Romano, E., Giudici, M., 2009. On the use of meteorological data to assess the evaporation from bare soil. J. Hydrol. 372, 30–40.

Rundel, P.W., Graham, E.A., Allen, M.A., Fisher, J.C., Harmon, T.C., 2009. Environmental sensor networks in ecological research. New Phytol. 182, 589–607 (Tansley review).

Saito, H., Simunek, J., 2009. Effects of meteorological models on the solution of the surface energy balance and soil temperature variations in bare soils. J. Hydrol. 373, 545–561.

Santanello, J.A., Friedl, M.A., 2003. Diurnal covariation in soil heat flux and net radiation. J. Appl. Meteorol. 42, 851–862.

Schnitzer, S.A., Dalling, J.W., Carson, W.P., 2000. The impact of lianas on tree regeneration in tropical forest canopy gaps: evidence for an alternative pathway of gap-phase regeneration. J. Ecol. 88, 655–666.

Schob, C., Kammer, P.M., Choler, P., Veit, H., 2009. Small-scale plant species distribution in snowbeds and its sensitivity to climate change. Plant Ecol. 200, 91–104.

Singh, A., Budzik, D., Chen, W., Batalin, M.A., Stealey, M., Borgstrom, H., Kaiser, W.J., 2006. Multiscale sensing, a new paradigm for actuated sensing of high frequency dynamic phenomena. In: Proceedings of the 2006 IEEE/RSJ International Conference on Intelligent Robots and Systems, Beijing, China, pp. 328–335.

Singh, A., Batalin, M.A., Chen, V., Stealey, M., Jordan, B., Fisher, J.C., Harmon, T.C., Hansen, M.H., Kaiser, W.J., 2007. Autonomous robotic sensing experiments at San Joaquin river. In: Proceedings of the 2007 IEEE International Conference on Robotics and Automation, Roma, Italy, pp. 4987–4993.

Slaughter, D.C., Giles, D.K., Downey, D., 2008. Autonomous robotic weed control systems: a review. Comput. Electron. Agric. 61, 63–78.

Suleiman, A., Crago, R., 2004. Evapotranspiration using radiometric surface temperatures. Agron. J. 96, 384–390.

Van Wijk, W.R., de Vries, D.A., 1966. Periodic temperature variations in a homogeneous soil. In: Van Wijk, W.R. (Ed.), Physics of Plant Environment, 2nd ed. North-Holland Publishing Company, Amsterdam, pp. 102–143.

Weiss, A., Hays, C.J., 2005. Calculating daily mean air temperatures by different methods: implications from a non-linear algorithm. Agric. For. Meteorol. 128, 57–65.

Zheng, D., Hunt Jr., E.R., Running, S.W., 1993. A daily soil temperature model based on air temperature and precipitation for continental applications. Clim. Res. 2, 183–191.